PLOS ONE

RESEARCH ARTICLE

Response of grassland ecosystem to monsoonal precipitation variability during the Mid-Late Holocene: Inferences based on molecular isotopic records from Banni grassland, western India

Sayak Basu[1¤]*, Prasanta Sanyal[1], Anusree A. S. Pillai[2,3], Anoop Ambili[1¤]

1 Indian Institute of Science Education and Research Kolkata, Mohanpur, West Bengal, India, **2** National Centre for Biological Sciences (NCBS), GKVK Campus, Bangalore, Karnataka, India, **3** Manipal Institute of Higher Education, Madhav Nahar, Manipal, Karnataka, India

¤ Current address: Indian Institute of Science Education and Research Mohali, Punjab, India
* sayak.geo@gmail.com

OPEN ACCESS

Citation: Basu S, Sanyal P, Pillai AAS, Ambili A (2019) Response of grassland ecosystem to monsoonal precipitation variability during the Mid-Late Holocene: Inferences based on molecular isotopic records from Banni grassland, western India. PLoS ONE 14(4): e0212743. https://doi.org/10.1371/journal.pone.0212743

Editor: Robert Hilton, Durham University, UNITED KINGDOM

Received: March 8, 2018

Accepted: February 8, 2019

Published: April 17, 2019

Data Availability Statement: All relevant data are within the paper and its Supporting Information files.

Funding: PS gratefully acknowledge financial support from the Department of Science and Technology, New Delhi (Project No. SB/S4/ES-684/2013). There was no additional external funding received for this study.

Competing interests: The authors have declared that no competing interests exist.

Abstract

Banni, located in the arid western India, is one of the largest tropical grasslands of the Asian continent. The net primary production in this grassland ecosystem is currently mediated by precipitation during the Indian summer monsoon (ISM). However, timing of the grassland expansion and its link to the intensity of monsoonal precipitation remains enigmatic due to the paucity of datasets. The major objective of this study is to understand the changes in monsoonal precipitation and vegetation for the last 4600 cal yr BP using hydrogen and carbon isotopic composition of *n*-alkanes ($\delta D_{n\text{-alkane}}$ and $\delta^{13}C_{n\text{-alkane}}$) measured from two core sediments (Chachi and Luna) in Banni region. The $\delta^{13}C_{C29}$ and $\delta^{13}C_{C31}$ values for Chachi core sediments vary from −30.9 ‰ to −27.2 ‰ and −34.4 ‰ to −25 ‰ respectively. The $\delta^{13}C_{n\text{-alkane}}$ values from the core sediments are converted into $\%C_4$ plants based on a binary mixing model using the end-member $\delta^{13}C_{n\text{-alkane}}$ values derived from the dominant modern vegetation in the Banni region. The prominent feature of the paleovegetation curve is the marked increase in the $\delta^{13}C_{n\text{-alkane}}$ values after 2500 cal yr BP, which suggests proliferation of C_4 grasses in this region. Similar changes after 2500 cal yr BP have also been observed in the $\delta D_{n\text{-alkane}}$ values. The δD_{C29} values are used to calculate δD value of paleoprecipitation that varied from 10 ‰ to −60.2 ‰. A significant increase in the δD values of paleoprecipitation (ca. 25 ‰) indicates a weakened ISM precipitation after ca. 2500 cal yr BP. The regional aridification and frequent fire events may have helped the expansion of C_4 plant dominated grassland ecosystem in Banni region. Correlation between paleoclimatic records suggests that the southward migration of intertropical convergence zone and more frequent warm phases of El-Nino Southern Oscillation have triggered the weakening of monsoonal precipitation in the tropical region.

Introduction

Grasslands are globally important as they comprise nearly one-fifth of the world's land surface and 80% of the total agriculturally productive land [1–2]. Geographical distribution, community composition and net primary production of grassland ecosystems not only play crucial roles in global carbon budget [3] but also influence regional climate by modulating the evapotranspiration flux [4]. The vegetation composition of grassland ecosystems reflects the competing influence of precipitation, fire and atmospheric CO_2 concentration. For instance, changes in CO_2 level and fire events in the grassland of West Africa during the Late Holocene shifted the vegetation composition towards woody plant cover, despite the increased regional aridity [5]. It is important to note that the interaction between above-mentioned forcing factors varies across the globe and thus produces a site-specific structure of the grassland ecosystem. Furthermore, the magnitude of the climatic factors and their effects on vegetation composition are also globally variable, depending upon duration of the rainy season, precipitation amount and number of precipitation events [6]. Prolonged and recurrent droughts predicted in a warming environment, combined with human-induced changes in the natural hydrological regime, will likely have an adverse effect on biodiversity of the grasslands [7, 8]. The understanding of past climate-ecosystem coupling is thus vital to predict future ecosystem response to changing natural variables.

The available Mid-Late Holocene paleoclimate records from Indian summer monsoon (ISM) domain suggest significant modifications in seasonal distribution of monsoonal precipitation in response to shifts of the Intertropical Convergence zone (ITCZ) [9–11]. Changes in hydrological regime will likely to have a major impact on the biodiversity of the Banni grasslands in western India—one of the largest tropical grassland of Asian continent. The modern day precipitation of Banni grassland is characterized by extremely sparse rain events (n = 10–12), short length of monsoon season and very high temperature difference (ca. 40 ˚C) between summer and winter months. This extreme climate setting makes the Banni grassland an ideal site to investigate the past climate-grassland interactions.

A previous study from the Banni grassland used the carbon isotopic composition of bulk organic matter ($\delta^{13}C_{org}$) and oxygen isotopic composition of gastropod shells ($\delta^{18}O_{shell}$) to decipher paleoenvironmental changes [12]. The $\delta^{13}C_{org}$ values from the Banni grassland suggested Late Holocene expansion of a C_4 grass dominated ecosystem in response to changes in moisture availability and local fire-events [12, 13]. However, $\delta^{13}C_{org}$ value based estimates of $\%C_4$ plants have uncertainties due to thermal degradation of selective organic compounds [14], which can alter the pristine isotopic character [15]. Furthermore, $\delta^{13}C_{org}$ values integrate organic matter from numerous sources (each with distinct $\delta^{13}C$ value) that can often led to bias in paleovegetation reconstruction [16]. Likewise, uncertainty has also been associated with $\delta^{18}O_{shell}$ based climate interpretation due to interplay of factors such as local precipitation variability, changes in the moisture pathway, lake water evaporation, residence time, temperature as well as biological effects controlling the $\delta^{18}O$ values [17]. Therefore, more robust hydrological and vegetational proxies are required for an improved assessment of the paleoenvironmental changes from this region.

To achieve a better understanding of the past vegetation composition and its linkage with climatic factors, the present study measured carbon and hydrogen isotopic composition of *n*-alkanes ($\delta D_{n\text{-alkane}}$ and $\delta^{13}C_{n\text{-alkane}}$) extracted from two seasonal wetland sediment cores (Chachi and Luna) (Fig 1). The relative phasing of vegetation and precipitation are assessed from the isotopic composition of same compound (i.e., *n*-alkane). Comparison of records from multiple seasonal wetlands provides a synoptic view of past environmental changes in this region. The objectives of the present study include (i) understanding the potential sources of organic

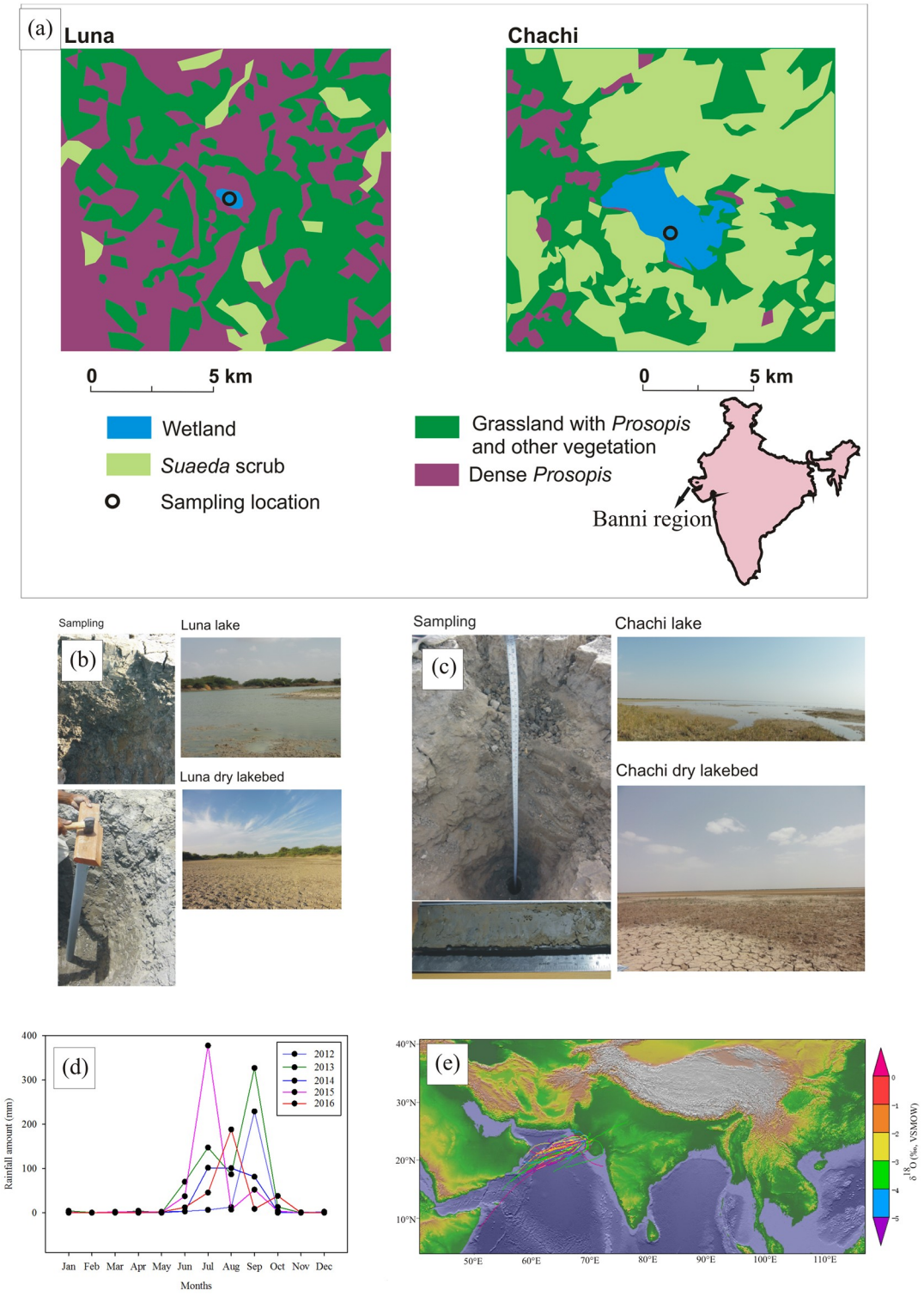

Fig 1. Study area, sampling and modern climate in Banni grassland. (A) Schematic representation of plant functional types around the seasonal wetlands [13, 18]. Images showing core sampling in (B) Chachi and (C) Luna wetlands. (D) Monthly precipitation in the Banni region for past 5 years. (E) Back-trajectory analysis of the air-parcel demonstrates that Arabian Sea is the dominant moisture contributor to the precipitation in Banni region.

https://doi.org/10.1371/journal.pone.0212743.g001

matter (OM) in the Banni region; (ii) reconstruction of the climatic conditions and local vegetation history; (iii) recognizing the spatial variability of ISM; (iv) interpreting the role of teleconnections on the intensity of ISM precipitation and; (v) understanding the feedback mechanism loop between monsoonal precipitation, fire and CO_2. To our best of knowledge, this is the first continuous biomarker-based record of climate change from western India during the Mid-Late Holocene.

Study area

Modern climate

The Banni terrain (total area: 3,847 km^2, 23˚19' to 23˚52' N and 68˚56' to 70˚32' E) is a flat transitional land which lies between the mainland Kachchh and the Great Rann, one of the world's largest hypersaline marshy area. This region accounts for 8.4% of the total area of Kachchh Desert, western India [19]. The Banni region receives the dominant fraction (80–90%) of annual precipitation (avg. 310 mm) during ISM (Fig 1D). The average seasonal temperature in this region varies from 50 ˚C in summer (May-July) to 10 ˚C in winter (December-February) [18].

Geomorphology

Banni, a tectonically raised mudflat, is located on the southern edge of the Great Rann of Kachchh [20]. This unique geomorphic terrain is slightly elevated (ca. 4 to 20 m) from the Great Rann with sediments comprising of fluvial origin [20]. The sediments in the Banni region are derived from the Mesozoic sedimentary rocks of northern Kachchh Mainland brought down by the north flowing drainage system comprising of Khari, Chhari and Kaila rivers [21–22]. The fine textured Banni sediments are composed of stratified silt and clay with thickness more than 30 m [23]. Soil salinity is highly variable, and pH ranges between 6.5 and 8.5 [23].

Modern vegetation

The modern-day vegetation in Banni region is characterized by the mixed C_3-C_4 plants [13] (Fig 1A). Vegetation of Banni comprises of herbs (89 species, accounts for ca. 46% of all the plant species), grasses (37 species, ca. 19% of all the plant species,) shrubs (31 species, ca. 16% of all the plant species), trees (17 species, ca. 9% of all the plant species), and sedges and climbers (ca. 10% of plant species) [24]. The Chachi site comprises of Suaeda scrub and grassy vegetation with sparse cover of *Prosopis juliflora* and other herbaceous vegetation, whereas the catchment of Luna is composed of grassland with moderate density of *Prosopis juliflora* [13]. The region is covered with coarse and low perennial grasses like the *Desmostachya bipinnata*, *Sporobolus marginatus*, *Dichanthium annulatum*, *Cenchrus ciliaris*, *Sporobolus fertilis* and *Chloris barbata* [25]. Prominent tree species of this region are *Acacia nilotica subsp. indica*, *Prosopis juliflora*, *Prosopis cineraria*, *Salvadora oleoides and Salvadora persica* [25]. The region is currently degraded mostly due to frequent droughts events coupled with intense grazing and invasion of *Prosopis juliflora* [19].

Methods

Field sampling

Core sediments were collected from two closed shallow seasonal wetlands (Chachi and Luna) during a field expedition in summer 2012 when the region was completely dried up (Fig 1B and 1C). The cores (ca. 138 cm and 85 cm depth for Chachi and Luna, respectively) were

retrieved using 6 cm diameter, long PVC pipes. No specific permissions were required for the sample collections from these locations. All the samples were stored at 4 ˚C before the analysis. The sediment cores collected from Chachi and Luna were clayey with occasional silt laminations [12]. The Chachi core was sub-sampled at 5–8 cm intervals until 70 cm depth followed by 4 cm intervals and Luna core was sub-sampled at 6 cm intervals. In addition to core sediment samples, leaf samples of dominant vegetation (grasses, herbs and trees) were also collected. The surface of the leaf samples were cleaned with 0.5 N HCl and distilled water in an ultrasonic bath to remove adhered contaminants. Leaf samples were dried at 40 ˚C for 48 hours, and core sediment samples were dried at 50 ˚C for 8 hours. Leaves and sediment samples were subsequently powdered in an agate mortar for further analysis. All the biomarker-based analyses were conducted at the stable isotope laboratory of Indian Institute of Science Education and Research Kolkata.

Extraction and analysis of *n*-alkane

Total lipid extract (TLE) is obtained via accelerated solvent extractor (Dionex, ASE350) using dichloromethane/methanol (93:7) mixture at 100 ˚C and 1600 psi pressure for 15 min (2 cycles). For this purpose, 0.3–0.5 g leaf and 7–8 g sediment samples were used. Sample preparation and lipid extraction methods have been described in detail elsewhere [12, 26, 27]. TLE fraction was concentrated in a Rotavapour (R-210, Buchi) by evaporating the dichloromethane and methanol mixture. The non-polar hydrocarbon fraction (*n*-alkane) was separated from the TLE using short-column silica gel column chromatography, using activated silica gel (100–200 mesh) in Pasteur pipette plugged with glass wool and hexane as eluent. Then *n*-alkane fraction has been concentrated up to 0.5 ml under a stream of dry N_2.

The concentration of individual *n*-alkane was measured in a gas chromatograph (Agilent 7890A, GC system) equipped with a split/splitless injector, non-polar capillary column (HP5-MS, 30 m × 250 μm × 0.25 μm) and flame ionized detector (FID). Samples were injected in 1:1 split mode with an initial inlet temperature of 320 ˚C. The GC oven temperature was started at 60 ˚C (held 2 min) and then increased to 320 ˚C at 8 ˚C/min (held 12 min). The characteristic retention time obtained from the external *n*-alkane standard mixture (SUPELCO C_8–C_{40} alkanes) was used for the identification and quantification of individual *n*-alkanes.

The δD and δ^{13}C analyses of *n*-alkane

For the Chachi core sediments, a total of 19 and 16 samples were measured for $\delta^{13}C_{n\text{-alkane}}$ and $\delta D_{n\text{-alkane}}$ values respectively. For Luna core sediments, $\delta^{13}C_{n\text{-alkane}}$ analysis has been carried out on 14 samples. All samples were not analyzed for $\delta D_{n\text{-alkane}}$ values compared to $\delta^{13}C_{n\text{-alkane}}$ due to limited sample material.

The $\delta^{13}C_{n\text{-alkane}}$ values were measured in Thermo Trace GC Ultra, connected via combustion interface (GC-Isolink) and Conflo IV interface to a MAT 253 isotope ratio mass spectrometer (GC-IRMS). The GC oven temperature was raised from 40 ˚C (held 1 min) to 320 ˚C (held 12 min) at 10 ˚C/min. 1 μl samples were injected in splitless mode with an inlet temperature at 280 ˚C and He as carrier gas at 1 ml/min. Individual compounds were combusted over Nickel and Copper wire in the presence of O_2 with He (1% v/v) at 950 ˚C to produce CO_2. Calibration of $\delta^{13}C_{n\text{-alkane}}$ value was performed by injecting several pulses of CO_2 at the beginning and the end of each GC run. Isotopic ratios are expressed in ‰ relative to the Vienna Pee Dee Belemnite (VPDB) standard. A standard mixture of *n*-alkanes (C_{16}-C_{30}) procured from Prof. Arndt Schimmelmann of Indiana University, with a known isotopic composition was used at different dilution (0.5, 1, 1.5, 7.5 and 15 ng/μl) to monitor the accuracy of the measurement.

The $\delta D_{n\text{-alkane}}$ values were measured using a Thermo Trace GC Ultra coupled via a GC Isolink pyrolysis interface operated at 1420 ˚C to a Thermo MAT 253 GC-IRMS. The $\delta D_{n\text{-alkane}}$ values were measured against calibrated H_2 reference gas. The $\delta D_{n\text{-alkane}}$ values are reported in ‰ notation against the Vienna Standard Mean Ocean Water (VSMOW). The Schimmelmann standard was used at different dilution (35, 50, 75 and 105 ng/μl) to assess the accuracy of the analysis. Long-term repeated analysis of the external standard mixture rendered a precision of ±3 ‰ (1σ) and an average accuracy of 1 ‰. The H_3^+ factor varied around 11.1 ± 0.02 ppm nA^{-1} throughout the measurement period.

Chronology

The published ^{14}C activity measurements made on bulk organic matter are used to constrain an age model for Chachi and Luna core sediments [12]. However, using the radiocarbon activity of bulk organic carbon to date the deposition of lake sediments is often hampered by i) the "reservoir effect", carbon in the organic fraction derived from old groundwater or dissolution of limestone [28, 29, 30]; (ii) contamination by reworked organic materials from weathering and erosion in the upstream catchment can dilute the ^{14}C content of organic materials with respect to the atmosphere at the time of deposition [31, 32]. The chronology based on the AMS dating of bulk organic sediments in Chachi and Luna core sediments are stratigraphically consistent [12]. The bulk organic matter in the Banni core sediments has dominant source derived from the terrestrial vascular plants [12] that incorporate ^{14}C in cellulose sourced from $^{14}CO_2$ in the atmosphere [33]. Therefore, the bulk organic matter in the Banni core sediments is relatively free of any "reservoir effect" making it an ideal material for applying ^{14}C to date the sediments. The ^{14}C dates were calibrated using OxCal 4.1 software [34] with the IntCal 09 calibration curve [35]. The average sedimentation rates of the Chachi and Luna sediments are 0.03 and 0.06 cm yr^{-1} respectively. The age-depth relationship was modeled using linear interpolation between adjacent radiocarbon measurements.

Quantification of organic source using *n*-alkane indices

The *n*-alkane indices have been used to obtain information on OM sources using the source-specific carbon chain length [36, 37]. The long-chain *n*-alkanes (C_{27}–C_{33}) tend to dominate terrestrial leaf waxes, short-chain *n*-alkanes less than C_{21} are more characteristic of algae, and mid-chain *n*-alkanes (C_{21}, C_{23}, and C_{25}) are mainly produced by aquatic macrophytes [38, 39].

In the present study, P_{aq}, Terrigenous versus aquatic ratio (TAR) and carbon preference index (CPI) have been calculated. The P_{aq} and TAR indices have widely been used to estimate the relative proportion of terrestrial flux in the sediments [39, 40].

Following equations have been used in this study:

$$\mathrm{Paq} = \frac{(C_{23} + C_{25})}{(C_{23} + C_{25} + C_{29} + C_{31})}$$

$$\mathrm{TAR} = \frac{(C_{27} + C_{29} + C_{31})}{(C_{15} + C_{17} + C_{19})}$$

$$\mathrm{CPI} = 0.5 \times \left[\frac{(C_{27} + C_{29} + C_{31} + C_{33})}{(C_{26} + C_{28} + C_{30} + C_{32})} + \frac{(C_{27} + C_{29} + C_{31} + C_{33})}{(C_{28} + C_{30} + C_{32} + C_{34})}\right]$$

[41].

Back-trajectory computation

The probable moisture source of the air masses has been deduced based on the backward trajectories computed from the database of the National Oceanic and Atmospheric Administration (NOAA, http://www.arl.noaa.gov/ready/hysplit4.html) using Hybrid Single-Particle Lagrangian Trajectories (HYSPLIT-4). Trajectories were computed for 48 hours at 500, 1500 and 2500 m.a.s.l. as precipitation in India is expected to originate from these altitudes [42]. In daily time-scale, trajectories did not show much variation with altitude, and hence 500 m.a.s.l. was considered to be cloud base height for precipitation over the Banni region.

The δD value of precipitation in Banni grassland

In the absence of meteorological station in Banni grassland, the Isotope Global Spectral Model version 2 (IsoGSM2) prediction of the stable isotopic composition of regional precipitation [43] has been used in the present study. This model provides monthly averaged δD and $\delta^{18}O$ values of precipitation for the years 2011 to 2015. The spatial resolution of the model is 1.9˚ latitude 1.8˚ longitude. In IsoGSM2, atmospheric processes and temperature fields are constrained by spectral nudging. The detailed description of the model has been provided elsewhere [43]. In this study, 5 years weighted averaged δD and $\delta^{18}O$ values of precipitation have been used as a reference dataset to interpret paleoclimatic signals.

Statistical analyses

The Mann-Whitney U test has been used to assess statistically significant differences between $\delta D_{n\text{-alkane}}$ and $\delta^{13}C_{n\text{-alkane}}$ values of the Chachi core sediments before and after 2500 cal yr BP. This test is commonly used to identify the significantly differing groups, which are not normally distributed [44]. The null hypothesis of this non-parametric test is that the difference of location between the samples is equal to zero, while the alternative hypothesis is that the difference of location between the samples is different to zero. The analysis has been conducted at a significance level of 95%. In this study, this analysis has been conducted on both δD_{C29} and δD_{C31} values for two time-slices; 4600 to 2500 cal yr BP and 2500 cal yr BP to present. Mann-Kendall trend analysis, a nonparametric test, has been employed to identify the trends in time-series of $\delta D_{n\text{-alkane}}$ and $\delta^{13}C_{n\text{-alkane}}$ values of the Chachi core sediments. The null hypothesis of this non-parametric test is that there is no trend in the time-series. The alternative hypothesis is that there is a trend in the time-series. The analysis has been conducted at a significance level of 95%. The correlation between dependent and independent variables has been calculated using linear regression analysis. All the statistical analyses have been conducted using PAST (Paleontological Statistics) and Sigma Plot software (version 12.5).

Results

Molecular level characterization of the OM

The *n*-alkane distributions in leaves of modern plants showed the dominance (ca. 80% of total concentration) of C_{29} and C_{31} homologues (S1 Fig). On the contrary, the *n*-alkanes distribution in the core sediments displayed a distinct bimodal distribution with carbon numbers ranging from C_{16}–C_{35} (S2 Fig). In the Chachi core sediments, total *n*-alkane concentration ranged from 120 μg g^{-1} to 700 μg g^{-1} and reached the maximal value at the topmost section of the core. The short-chain and long-chain *n*-alkanes accounted for ~ 40% and ~25% of the total *n*-alkane concentration respectively. The CPI values for the Chachi and Luna core sediments varied from 2.9 to 15.7 (Fig 2A) and 3.2 to 4.2 respectively. The P_{aq} values for the Chachi and Luna core sediments varied from 0.07 to 0.33 (Fig 2B) and 0.10 to 0.25, respectively. The TAR

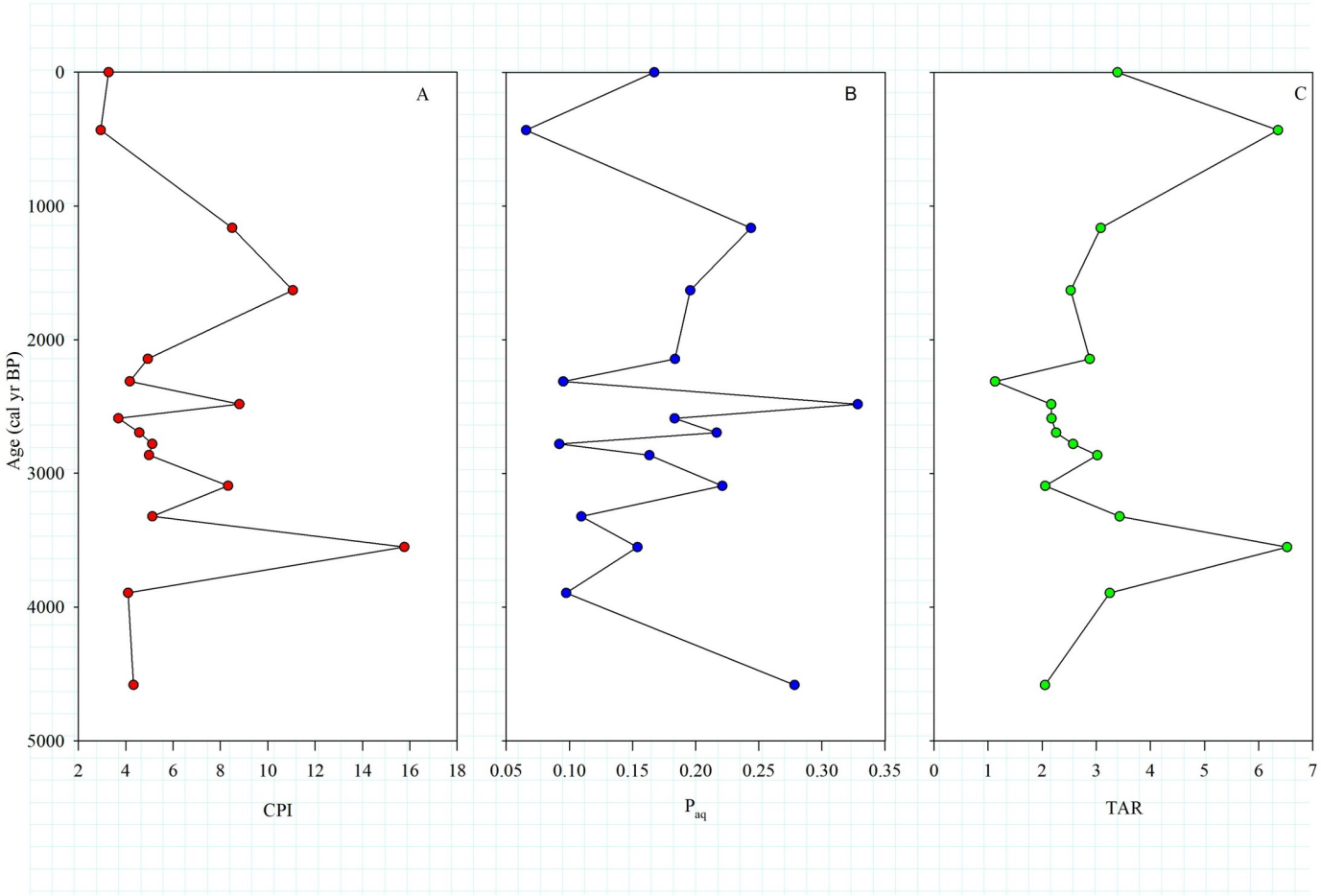

Fig 2. Down core profile of *n*-alkane indices in Chachi core sediments. (A) CPI, (B) P_{aq}, and (C) TAR values for the Chachi core sediments.

https://doi.org/10.1371/journal.pone.0212743.g002

Table 1. Compound specific δD and $\delta^{13}C$ values for the long chain *n*-alkanes of modern vegetation from Banni region. SD = standard deviation (1σ).

	Sample	$\delta^{13}C_{C29}$ (‰, VPDB)	S.D.	δD_{C29} (‰, VSMOW)	S.D.	$\delta^{13}C_{C31}$ (‰, VPDB)	S.D.	δD_{C31} (‰, VSMOW)	S.D.
C_3 plants	*Solanum viarum*	-34.9	0.4	-122	4	-37.4	0.3	-198	2
	Mangifera indica	-34.9	0.4	-173	2	-37.2	0.3	-184	3
	Eupatorium odoratum	-32.7	0.2	-133	3	-37.6	0.3	-141	2
	Salvadora persica	-30.1	0.8	-116	4	-30.7	0.5	-132	1
	Acacia nilotica	-36.1	0.3	-165	5	-36.1	0.4	-189	2
	Azadirachta indica	-33.4	0.1	-141	4	-33.6	0.2	-154	3
	Physalis minima	-34.0	0.3	-123	3	-36.9	0.4	-143	1
	Citrus lemon	-32.6	0.4	-98	4	-35.0	0.3	-160	1
	Average	**-33.6 ± 1.8**		**-133 ± 25.1**		**-35.5 ± 2.4**		**-162 ± 24.7**	
C_4 plants	*Cenchrus ciliaris*	-21.0	0.5	-218	4	-22.2	0.3	-150	2
	Chloris barbata	-22.8	0.3	-144	3	-23.7	0.4	-177	1
	Panicum miliaceum	-22.1	0.3	-177	1	-24.4	0.4	-209	4
	Suaeda fruticosa	-21.9	0.4	-187	4	-21.9	0.5	-219	4
	Desmostachya bipinnata	-23.9	0.3	-155	2	-25.8	0.2	-169	2
	Average	**-22.4 ± 1.1**		**-176 ± 28.9**		**-23.6 ± 1.6**		**-185 ± 28.6**	

https://doi.org/10.1371/journal.pone.0212743.t001

Table 2. δD and $\delta^{13}C$ values for the long chain *n*-alkanes of Chachi core sediments N.A. = not available/not determined. SD = standard deviation (1σ).

Sample	Depth	Age cal yr BP	$\delta^{13}C_{C29}$ (‰, VPDB)	S.D.	$\delta^{13}C_{C31}$ (‰, VPDB)	S.D.	δD_{C29} (‰, VSMOW)	S.D.	δD_{C31} (‰, VSMOW)	S.D.
Chachi sediments										
Ca-1	0	0	-28.3	0.4	-28.7	0.1	-77	2	-93	4
Ca-2	8	471	-27.9	0.2	-26.2	0.0	N.D.		N.D.	
Ca-4	20	1177	-27.5	0.4	-27.2	0.3	-77	3	-72	0
Ca-8	40	1631	-27.6	0.1	-25.0	0.2	-71	2	-83	2
Ca-12	60	1844	-27.2	0.4	-26.8	0.2	-97	0	-108	0
Ca-15	74	2140	-28.7	0.3	-27.9	0.7	-106	4	-98	2
Ca-17	82	2310	-29.2	0.2	-28.0	0.2	-88	0	-90	3
Ca-19	90	2480	-29.3	0.2	-29.4	0.8	N.D.		N.D.	
Ca-20	95	2586	-29.7	0.5	-31.7	0.4	-104	4	-116	2
Ca-21	100	2692	-28.1	0.0	-28.9	0.1	-96	1	-116	2
Ca-22	104	2777	-27.2	0.2	-27.3	0.4	-121	2	-107	3
Ca-23	108	2862	-28.4	0.2	-28.8	0.9	N.D.		N.D.	
Ca-24	112	3090	-29.9	0.1	-30.0	0.4	-99	2	-113	1
Ca-25	116	3319	-28.5	0.2	-29.9	1.0	-129	1	-126	4
Ca-26	120	3548	-30.9	0.2	-34.4	0.5	-113	1	-124	1
Ca-27	126	3892	-29.0	0.2	-31.3	0.2	-121	7	-121	2
Ca-28	130	4121	-29.5	0.1	-30.2	0.6	-115	5	-129	2
Ca-29	134	4350	-30.3	0.6	-29.8	0.1	-122	4	-134	1
Ca-30	138	4578	-29.1	0.1	-31.3	0.3	-110	2	-132	3

https://doi.org/10.1371/journal.pone.0212743.t002

values of the Chachi sediments ranged from 1.1 to 6.5 (Fig 2C), whereas the Luna core sediments varied from 4.1 to 5.1.

The *δ*D and $\delta^{13}C$ values of long-chain *n*-alkane in modern plants

The $\delta D_{n\text{-alkane}}$ and $\delta^{13}C_{n\text{-alkane}}$ values of the modern vegetation from Banni region are listed in Table 1. The modern C_3 vegetation in Banni region showed average $\delta^{13}C_{C29}$ value of −33.6 ± 1.8 ‰ and $\delta^{13}C_{C31}$ values of −35.5 ± 2.4 ‰ (n = 8, 1σ). The average $\delta^{13}C_{C29}$ and $\delta^{13}C_{C31}$ values of modern C_4 plants are −22.4 ± 1.1 ‰ and −23.6 ± 1.6 ‰ (n = 5, 1σ) respectively. In C_3 plants, δD_{C29} and δD_{C31} values varied from −173 ‰ to −98 ‰ (avg = −133 ± 25.1 ‰) and −198 ‰ to −132 ‰ (avg = −162 ± 24.7 ‰). The δD_{C29} and δD_{C31} values of C_4 plants ranged between −218 ‰ to −144 ‰ (avg = −176 ± 28.9 ‰) and −219 ‰ to −150 ‰ (avg = −185 ± 28.6 ‰), respectively.

The $\delta^{13}C$ value of long-chain *n*-alkanes in core sediments

The $\delta^{13}C_{C29}$ and $\delta^{13}C_{C31}$ values of the Chachi core sediments varied from −30.9 ‰ to −27.2 ‰ and −34.4 ‰ to − 25.0 ‰ respectively (Table 2). The $\delta^{13}C_{n\text{-alkane}}$ values of both the homologues showed more negative values during 4600 to 2500 cal yr BP (Fig 3A). Afterwards, $\delta^{13}C_{C31}$ values displayed a progressively increasing trend with maximum values at 1500 cal yr BP. Similar trends are also observed for the $\delta^{13}C_{C29}$ values. The $\delta^{13}C_{C29}$ and $\delta^{13}C_{C31}$ values of the Chachi core sediments exhibit strong and significant positive correlation ($R^2 = 0.66$, $p < 0.05$). The p-values of Mann-Kendall analyses for the both homologues are less than 0.05 and Kendall's tau value for $\delta^{13}C_{C29}$ and $\delta^{13}C_{C31}$ values are 0.45 and 0.61. The $\delta^{13}C_{n\text{-alkane}}$ values of Luna core sediments for the last ca. 1000 parallels the Chachi record (Fig 3). The $\delta^{13}C_{C29}$ and $\delta^{13}C_{C31}$ values of the Luna core sediments ranged from –25.3 to –27.7 ‰ and –23.9 to –28.0 ‰ respectively (Table 3).

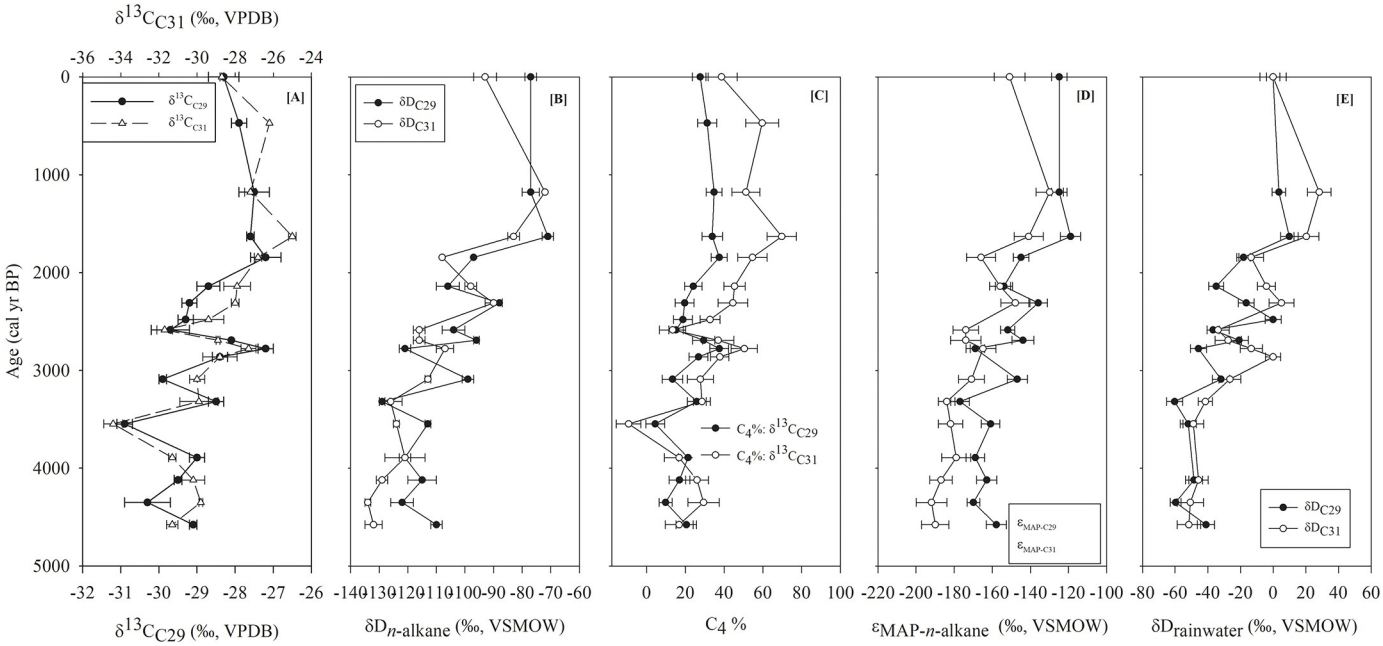

Fig 3. The isotopic profile and related calculations from the core sediments. [A] $\delta^{13}C_{n\text{-alkane}}$ and [B] $\delta D_{n\text{-alkane}}$ values for both n-C_{29} and n-C_{31} homologues. [C] Down-core calculated fractional C_4 contributions from both n-C_{29} and n-C_{31} homologues. [D] Down-core apparent hydrogen isotopic fractionation (ε_{app}) for each homologue calculated using the measured end-member compositions and calculated fractional C_4 contributions. [E] Down-core reconstructed $\delta D_{rainwater}$ values using the measured $\delta D_{n\text{-alkane}}$ and calculated ε_{app} values for each homologue. The horizontal lines in the figure represent the error associated with the calculations.

https://doi.org/10.1371/journal.pone.0212743.g003

The δD values of long-chain *n*- alkanes in core sediments

The p-values of Mann-Kendall analyses for the both homologues are less than 0.05 and Kendall's tau value for δD_{C29} and δD_{C31} values are 0.72 and 0.76, respectively. The magnitudes of fluctuation in δD values were similar for both C_{29} and C_{31} homologues (Table 2). In most of the samples, the δD_{C29} values were more positive compared to δD_{C31} value. The most prominent feature of the curve is the shift towards positive values after 2500 cal yr BP (Fig 3B). Accordingly, we have compared the values for two time-slices; 4600–2500 cal yr BP (phase-1) and 2500 cal yr BP to present (phase-2). The average δD_{C29} and δD_{C31} values during the phase-1 were −113.0 ± 10.7 ‰ and −121.8 ± 8.8 ‰ (n = 10, 1σ) respectively. The average δD_{C29} and δD_{C31} values during phase-2 were −86.0 ± 13.5 ‰ and −90.7 ± 12.3 ‰ (n = 6, 1σ). The difference in the δD_{C29} (and δD_{C31}) values for phase-1 and phase-2 has also been exhibited by Mann-Whitney test statistics. For both the homologues, we have found the p-values are less than significance level of 0.05 and thus reject the null hypothesis.

The stable isotopic composition of modern precipitation in Banni region

Monthly-weighted averaged δD values are positively correlated ($R^2 = 0.9$, $p < 0.05$) with the $\delta^{18}O$ values of precipitation. The Local Meteoric Water Line for the Banni region is:

$$\delta D = 7.6 \times \delta^{18}O + 7.9$$

(Fig 4A)

Due to the significant correlation ($R^2 = 0.9$), only the results of δD values of precipitation are further discussed. During 2011 to 2015, the δD values of precipitation varied from −4 ‰ to −77 ‰, and lower δD values coincide with the peak ISM precipitation (Fig 4B).

Table 3. $\delta^{13}C$ values for the long chain *n*-alkanes of Luna core sediments. SD = standard deviation (1σ).

Lune sediments						
Sample	Depth	Age cal yr BP	$\delta^{13}C_{C29}$ (‰, VPDB)	S.D.	$\delta^{13}C_{C31}$ (‰, VPDB)	S.D.
Lb-1	3	10	-27.2	0.1	-27.5	0.1
Lb-2	9.5	109	-26.6	0.4	-27.3	0.5
Lb-3	15.5	274	-26.3	0.6	-25.8	0.8
Lb-4	21.5	438	-27.6	0.2	-28	0.4
Lb-5	27.5	603	N.D			N.D
Lb-6	33.5	670	-25.7	0.3	-25.9	0.1
Lb-7	39.5	737	-27.4	1.1	-27.7	0.3
Lb-8	45.5	804	-26.6	0.1	-26.2	0.7
Lb-9	51.5	871	-26.3	0.1	-25.9	0.3
Lb-10	57.5	937	-26.2	0.7	-26.6	0.6
Lb-11	62.5	951	-27.7	0.3	-27.5	0.1
Lb-12	67.5	962	-25.3	0.0	-23.9	0.5
Lb-13	72.5	973	N.D		N.D	
Lb-14	77.5	984	-25.8	0.6	-25.3	0.4
Lb-15	82.5	995	-27.3	0.2	-27.9	0.6

https://doi.org/10.1371/journal.pone.0212743.t003

Discussion

Sources of organic matter

The *n*-alkane assemblage in the sediments is an effective biomarker tool for evaluating sources of organic matter due to the distinct carbon chain-lengths of terrestrial higher plants and microorganisms [26, 45]. In general, cuticular waxes of higher plants have a strong odd over even predominance in the long-chain *n*-alkanes and show CPI values >1, whereas the bacteria and algae are characterized by weak odd over even predominance and produce low CPI values (~1) [38]. Terrestrial higher plants are characterized by relatively higher abundances of odd-

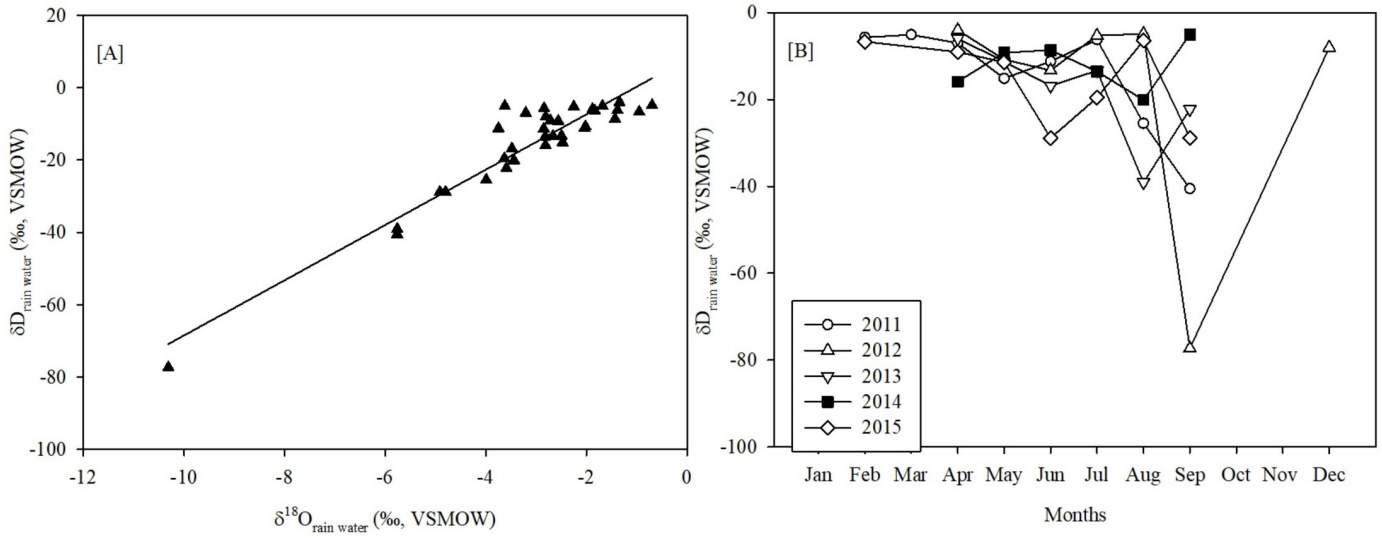

Fig 4. Isotopic variation of modern regional precipitation (IsoGSM2). (A) Local meteoric water line in the Banni region has been obtained using cross-plot between δD and $\delta^{18}O$ values. (B) The monthly averaged δD values of precipitation become progressively depleted in heavier isotope with the establishment of the ISM.

https://doi.org/10.1371/journal.pone.0212743.g004

numbered long-chain *n*-alkanes, whereas microorganisms contribute short-chain *n*-alkanes [16, 36]. In Banni core sediments, the higher abundance of the short-chain *n*-alkanes (S2 Fig) indicates a significant contribution from microorganisms to the *n*-alkane pool in the sediments. On the other hand, peaks observed in the long-chain *n*-alkanes maximise at C_{29} and C_{31}. The CPI values of both the sediment cores are consistent with the modern higher plants growing in the Indian subcontinent [27]. High CPI values (Fig 2A) suggest that long-chain *n*-alkanes in the sediments were derived from terrestrial higher plants. Further, the low P_{aq} values of Chachi core sediment indicate higher contribution of terrestrial biomass to the organic matter compared to aquatic productivity, and this observation is concordant with the TAR values (Fig 2B and 2C). Therefore, the long-chain $\delta^{13}C_{n\text{-alkane}}$ values would be suitable for the paleovegetational reconstruction.

Estimates of shifts from C_3 to C_4 plant type

A previous study from Banni grassland using bulk $\delta^{13}C_{org}$ values showed that $\%C_4$ plant varied from 16% to 43% [12] (S1 Table). However, bulk $\delta^{13}C_{org}$ values reflect contribution from multiple organic matter sources [16, 27], which are characterized by distinct isotopic composition. Furthermore, C_4 plant derived components degrades faster compared to its C_3 counterpart [46]. Therefore, paleovegetation reconstruction using the $\delta^{13}C_{org}$ values may provide an erroneous estimate of $\%C_3$-C_4 plants. The $\delta^{13}C_{n\text{-alkane}}$ values can refine the interpretation of bulk $\delta^{13}C_{org}$ data due to its resistance to biodegradation. Result of linear regression analysis shows that the $\delta^{13}C_{C29}$ and $\delta^{13}C_{C31}$ values of the Chachi core sediments exhibit a strong and significant positive correlation ($R^2 = 0.66$, $p < 0.05$). The large spread in the $\delta^{13}C_{C29}$ and $\delta^{13}C_{C31}$ values (Fig 3A) shows substantial variations in the vegetation composition. The $\delta^{13}C_{n\text{-alkane}}$ values are not only governed by the vegetation composition but also by physiological changes against moisture stress and $\delta^{13}C$ value of atmospheric CO_2 ($\delta^{13}C_{atmospheric\ CO2}$) [42, 47, 48]. The results from the Indian subcontinent show that $\delta^{13}C$ values of C_3 plants change only −0.4 ‰ for every 100 mm increase in the precipitation amount [49]. Therefore, ca. 2350 mm change in the annual precipitation would be required to explain the observed spread in the $\delta^{13}C_{C31}$ values (Table 2). Thus, we exclude moisture stress on the $\delta^{13}C_{n\text{-alkane}}$ values as the estimated precipitation change in the region seems unrealistic. The $\delta^{13}C_{atmospheric\ CO2}$ value has been declining rapidly in the recent decades as a consequence of the Suess effect (http://cdiac.ornl.gov/trends/co2/iso-sio/iso-sio.html). The modern $\delta^{13}C_{atmospheric\ CO2}$ value (−8.2 ‰) is 1.7 ‰ lower compared to that in the Mid-Late Holocene period [47], and accordingly the end-member $\delta^{13}C_{n\text{-alkane}}$ values of modern plants are corrected. The $\delta^{13}C_{n\text{-alkane}}$ values are converted into $\%C_4$ plants based on mixing model, where end-member values are the average isotopic composition of the dominant C_3-C_4 plants in Banni region (Table 1).

In the core sediments, the $\delta^{13}C_{C31}$ values correspond to 13% to 70% abundance of C_4 plants, while $\delta^{13}C_{C29}$ values indicate 5% to 38% abundance of C_4 plants (Fig 3C). Chemotaxonomic investigations showed that C_4 grasses in the savannah region synthesize more C_{31}, whereas C_{29} is the dominant homologue in C_3 dicots (S1 Fig) [50, 51]. The $\delta^{13}C_{C29}$ and $\delta^{13}C_{C31}$ values in the core sediments are believed to represent two distinct organic matter sources. Accordingly, in the present study, it has been assumed that $\delta^{13}C_{C29}$ values of the sediment samples reflect the changes in the abundance of C_3 trees, whereas $\delta^{13}C_{C31}$ values indicate the changes in $\%C_4$ grasses. The measured $\delta^{13}C_{C31}$ values provide higher estimation of C_4 plants compared to both $\delta^{13}C_{org}$ and $\delta^{13}C_{C29}$ values (Fig 3C, S1 Table). Therefore, it can be suggested that the $\delta^{13}C_{C31}$ values would be a more suitable proxy to infer vegetation change in the grassland setting.

Table 4. %C_4 plants calculated using $\delta^{13}C_{C29}$ and $\delta^{13}C_{C31}$ values of the Chachi core sediments.

Sample Number	Age (cal yr BP)	C_4% ($\delta^{13}C_{C29}$)	Uncertainty	C_4% ($\delta^{13}C_{C31}$)	Uncertainty
Ca-1	0	27.7	4.1	38.7	8.0
Ca-2	471	31.3	4.9	59.7	8.5
Ca-4	1177	34.8	4.1	51.3	7.2
Ca-8	1631	33.9	5.3	69.7	7.6
Ca-12	1844	37.5	4.1	54.6	7.6
Ca-15	2140	24.1	4.5	45.4	5.5
Ca-17	2310	19.6	4.9	44.5	7.6
Ca-19	2480	18.8	4.9	32.8	5.1
Ca-20	2586	15.2	3.7	13.4	6.7
Ca-21	2692	29.5	5.7	37.0	8.0
Ca-22	2777	37.5	4.9	50.4	6.7
Ca-23	2862	26.8	4.9	37.8	4.7
Ca-24	3090	13.4	5.3	27.7	6.7
Ca-25	3319	25.9	4.9	28.6	4.3
Ca-26	3548	4.5	4.9	-9.2	6.3
Ca-27	3892	21.4	4.9	16.8	7.6
Ca-28	4121	17.0	5.3	26.1	5.9
Ca-29	4350	9.8	3.3	29.4	8.0
Ca-30	4578	20.5	5.3	16.8	7.2

https://doi.org/10.1371/journal.pone.0212743.t004

The $\delta^{13}C_{C31}$ value-based calculation indicates ca. 20% higher abundance of C_4 plant during phase-2 compared to phase-1 (Table 4). Estimate of lower %C_4 plant till 2500 cal yr BP is concurrent with the pollen and phytolith records which showed the dominance of woody taxa (i.e., C_3 plants) during this interval [13]. The $\delta^{13}C_{n\text{-alkane}}$ values from the Luna core sediments for the last 1000 cal yr BP also shows high %C_4 plants in the Banni region. The trend in the $\delta^{13}C_{n\text{-alkane}}$ values corresponds well with the vegetation record from central India [42].

δD_{C29} value as a proxy for paleoprecipitation

The $\delta D_{n\text{-alkanes}}$ values from plant leaf wax have been increasingly used for the reconstruction of paleohydrological conditions [52–54]. The δD variability in leaf *n*-alkanes are mostly explained in terms of the changes in the δD values of regional meteoric water [54–59]. In addition, plant functional types and photosynthetic pathways can also affect the $\delta D_{n\text{-alkane}}$ values [60–63]. In the Chachi core sediments, the δD_{C29} values differ by -14 ‰ to 22 ‰ to the δD_{C31} values of the same sample. Difference sources of *n*-alkane can be assumed to explain this offset [64] as net apparent hydrogen fractionation between source water (i.e., MAP) and lipid ($\varepsilon_{MAP\text{-}n\text{-alkane}}$) of C_3 dicots is ca. 30 ‰ more positive compared to that of C_4 grasses [65].

Results from Banni grassland also show that $\varepsilon_{MAP\text{-}C29}$ value for C_3 plant is −113±25.1 ‰ while for C_4 plant the value is −156±28.9 ‰ (Table 1). Similar differences have been inferred from C_{31} homologue as well. The difference in water absorption systems in plant forms plays an important role that cause more negative δD values in *n*-alkanes from grasses than those from woody plants. The grasses (C_4) in the open ecosystem utilize water from deeper water sources (due to greater rooting depth of perennial grasses) compared to trees (C_3) in woodland setting as woody plants draw most of their water from soil surface through radial and shallow roots [65]. The different water-usage strategies of C_3 and C_4 plants may lead to a significant offset in the $\varepsilon_{MAP\text{-}n\text{-alkane}}$ (as well as $\delta D_{n\text{-alkane}}$) values and required to be addressed when the vegetation changes are large (as in the case of the present study).

In this study, the proportion of C_4 plants for each time-point has been calculated from the $\delta^{13}C_{C29}$ and $\delta^{13}C_{C31}$ values of the sediment samples (Table 3). Using the $\delta^{13}C_{n\text{-alkane}}$ based estimates of vegetation changes, the weighted averaged apparent fractionation factor between $\delta D_{n\text{-alkane}}$ and the $\delta D_{precipitation}$ ($\varepsilon_{n\text{-alkane-precip}}$) has been estimated using the following equation;

$$\varepsilon_{n-alkane-precip} = A \times \varepsilon_{n-alkane-precip(C_3 plants)} + (100 - A) \times \varepsilon_{n-alkane-precip(C_4 plants)}$$

Where, A is the $\%C_3$ plants. The weighted averaged $\varepsilon_{n\text{-alkane-precip}}$ values for each time-point have been presented in Fig 3D. Before the estimation of $\delta D_{precipitation}$ values, it is required to calculate the hydrogen isotopic fractionation during organic matter transport from leaf-wax to soil. Using the above-mentioned equation, the $\delta D_{n\text{-alkane}}$ value of modern leaf would be −125 ‰. On the other hand, the δD_{C29} value of the core-top sediment is −78 ‰, indicating incorporation of *n*-alkane into soil resulted in ca. 47 ‰ increase of the δD_{C29} value. Accordingly, the $\delta D_{n\text{-alkane}}$ values for each time-point have been corrected [66]. The δD value of regional precipitation has been calculated using the following equation [67];

$$\delta D_{precipitation} = \left[\frac{(\delta D_{n-alkane(corrected)} + 1000)}{(\varepsilon_{n-alkane-prec}/1000) + 1)} - 1000 \right]$$

The correlation analyses have been conducted between $\delta^{13}C$ and δD values of both the homologues for further interpretation of paleohydrological conditions. Results of the linear regression analysis have shown strong and significant positive correlation ($R^2 = 0.58$, $p < 0.05$, Fig 5) between δD_{C31} and $\delta^{13}C_{C31}$ values. The vegetation change as primary driver of hydrogen isotopic variability of C_{31} homologue can result in negative correlation between $\delta^{13}C_{C31}$ and δD_{C31} values. In contrast, the positive correlation indicates that the vegetation change has not influenced the hydrogen isotopic variations in C_{31} homologue. It has been further observed that the correlation between δD and $\delta^{13}C$ values for C_{29} homologue is weaker and insignificant ($R^2 = 0.15$, $p = 0.13$, Fig 5) suggesting that the δD values of this homologue are not influenced by the change from C_3 plants to C_4 grass [53]. Therefore, the $\delta D_{n\text{-alkane}}$ values of both the homologues can be used as a surrogate to understand the paleohydrological conditions. In this study, the further discussion is based on the δD_{C29} values. The $\delta D_{precipitation(C29)}$ values found to vary between 10 ‰ to −60.2 ‰ (Fig 3C).

In the low latitude tropical region, $\delta D_{precipitation}$ values are negatively related to the precipitation amount (i.e., amount-effect) and this inverse correlation is often used to explain the variations in the $\delta D_{n\text{-alkanes}}$ values [50, 51, 68, 69]. Instrumental record and back-trajectory computation of air-parcel show that precipitation in the Banni grassland is strongly seasonal (Fig 1D and 1E) with the dominant moisture contribution received from Arabian Sea. The seasonal difference in the net advection of moisture is reflected in the $\delta D_{precipitation}$ values (Fig 4B). Seasonal precipitation amount peaks during ISM months and coincides with low $\delta D_{precipitation}$ values, which indicates more negative δD_{C29} value of the sediment samples are representatives of high monsoonal precipitation events and vice-versa.

Paleohydrological changes in Banni grassland

More negative δD_{C29} values till 2500 cal yr BP suggest an enhanced monsoonal precipitation in Banni. Little fluctuations (max. 10 ‰) show that the region had experienced minor changes in the precipitation amount during phase-1. Relatively stable and high precipitation during this phase accompanied by higher $\%C_3$ plants (Fig 3C). After 2500 cal yr BP, the δD_{C29} values gradually shift towards more positive values, and the aridification peaked around 1500 cal year

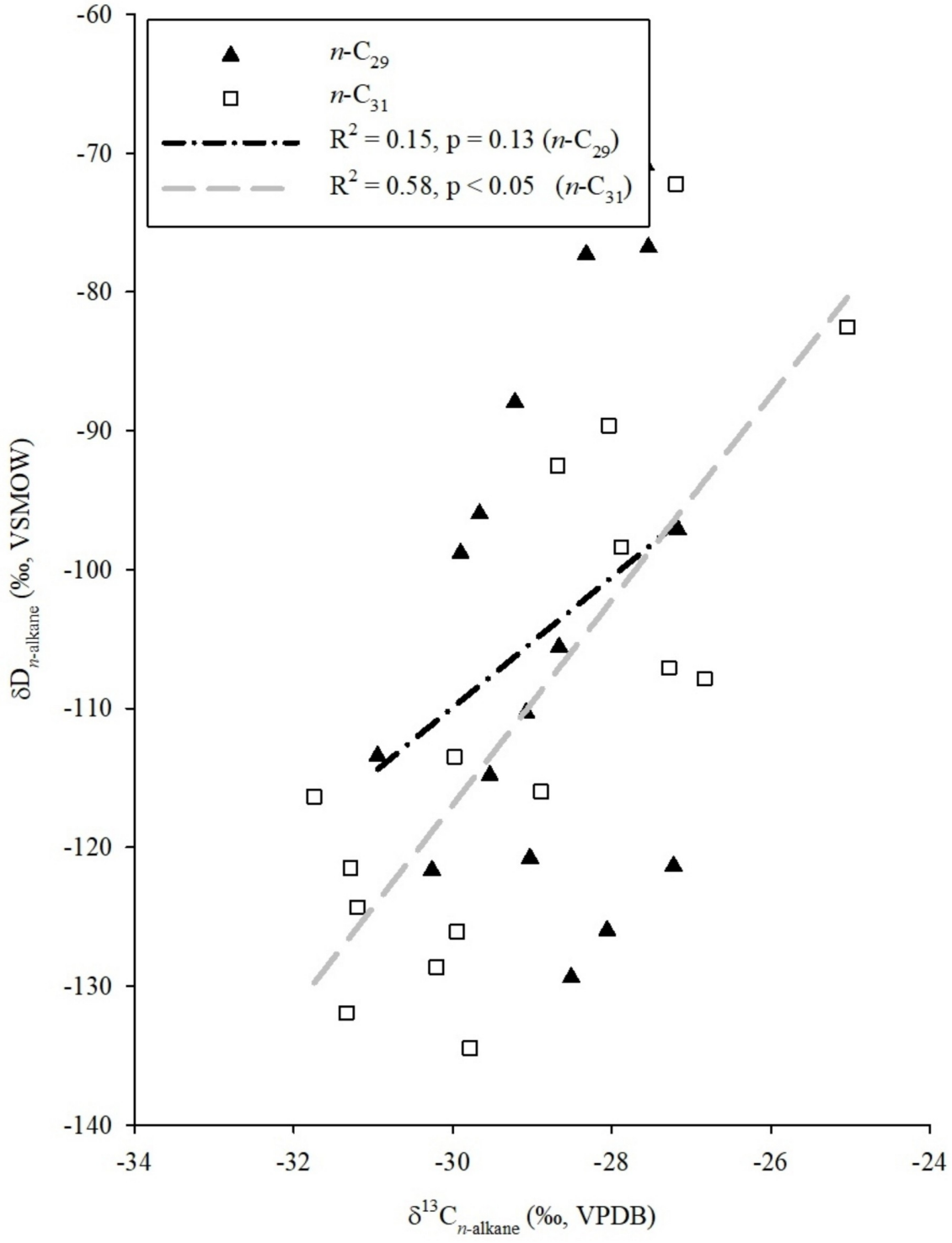

Fig 5. Regression analyses between $\delta D_{n\text{-alkane}}$ and $\delta^{13}C_{n\text{-alkane}}$ values for C_{29} and C_{31} homologues. Poor correlation (blue line) between the $\delta D_{n\text{-alkane}}$ and $\delta^{13}C_{n\text{-alkane}}$ values for C_{29} homologue indicates limited control of vegetation composition on the $\delta D_{n\text{-alkane}}$ values. Strong and significant positive correlation (red line) between the δD and $\delta^{13}C_{n\text{-alkane}}$ values for C_{31} homologue also suggests that change in vegetation type does not have influence on the $\delta D_{n\text{-alkane}}$ values in collected samples.

https://doi.org/10.1371/journal.pone.0212743.g005

BP. Regional aridity is also marked with the higher abundance of C_4 grasses during this interval (Fig 3C). A negative excursion (ca. 10 ‰) after 1000 cal yr BP shows a slight increase in precipitation amount in the Banni region towards the present. Overall, it can be suggested that the Banni region had experienced a gradual shift from more mesic to more arid condition since the last 4600 cal yr BP. The δD_{C29} value based record is consistent with the interpretation made from $\delta^{18}O_{shell}$ values in Banni core sediments [12].

Critical role of fire, CO_2 and precipitation on grassland stability

In general, low CO_2 condition and frequent fire events promote higher $\%C_4$ grasses at the expense of C_3 woody plant cover [70]. According to the CO_2 crossover model [71], Banni with temperature > 30 ˚C, the threshold atmospheric CO_2 level favoring C_4 plants over C_3 plants should be below 300 ppmv. The pCO_2 reconstruction for the studied period showed that atmospheric CO_2 level increased from 268 ppmv to 282 ppmv, a range favorable for the expansion of C_4 plants. However, the trend of C_4 plant expansion in Banni does not mimic the paleo-pCO_2 curve and exhibits an anti-phase relationship in between 2500 to 1500 cal yr BP (S3 Fig). Therefore, pCO_2 level alone cannot be attributed to the changing vegetation composition in Banni for the last 4600 cal yr BP.

The present study, in combination with published records, has attributed the increasing $\%C_4$ plants to the feedback mechanism between aridity, fire and vegetation composition. Increasing fire events (evidenced from Charcoal accumulation rate (CHAR)) from 2500 to 1500 cal yr BP helped to reduce C_3 woody plant cover and favored the expansion of C_4 grasses (S3 Fig). These fire events also promoted an arid understory microclimate and resulted in further drying in Banni. Continuous aridification helped fuel drying and led to more frequent fire events. In a nutshell, these effects have been enhanced by biogeophysical feedbacks; well-developed grasslands can favour the expansion of grasses by increasing light availability, reducing humidity and keeping high temperatures, all of which promote the growth of C_4 plants and are capable of maintaining the grassland setting.

Expansion of C_4 grasses can also impact the isotopic composition of the regional precipitation. Both IsoGSM2 model predictions and $\delta D_{n\text{-}alkane}$ value reveal extremely high precipitation δD values from Banni region. The present study suggests the following mechanism to explain this distinct isotopic character: the transpiration of grasses is higher compared to forest trees [72, 73]. Although transpiration is a non-fractionation process, it indeed enriches the atmospheric vapor in heavier isotopes [73] and resultant precipitation has more positive isotopic composition.

Regional comparison of climate data

The variations in precipitation in Banni grasslands for the last 4600 cal yr BP correspond well with published records from the ISM realm (Fig 6). The enhanced ISM precipitation in Banni during ca. 4600–2500 cal yr BP was synchronous with pollen and phytolith based investigations from Pariyaj lake in western India [74]. The geochemical proxies measured from the sediment core of an active mudflat of Diu Island in western India also indicate warm and humid conditions between 4105 and 2640 cal yr BP [75]. The results from Banni grassland are also corroborated by the geochemical and palynological analyses of relict mudflat from southern Saurashtra coast with wet climatic conditions and simultaneous occurrence of marginally high sea-level between 4710 and 2825 cal yr BP [76]. Likewise, the climatic reconstructions based on lake sediments from Nal Sarovar, central Gujarat [77] and Lunkaransar and Didwana Lakes of Rajasthan, western India [78, 79] observed a high lake stand during ca. 4680 and 3500 cal yr BP. The wetter conditions in Banni region during 4600–2500 cal yr BP is in good

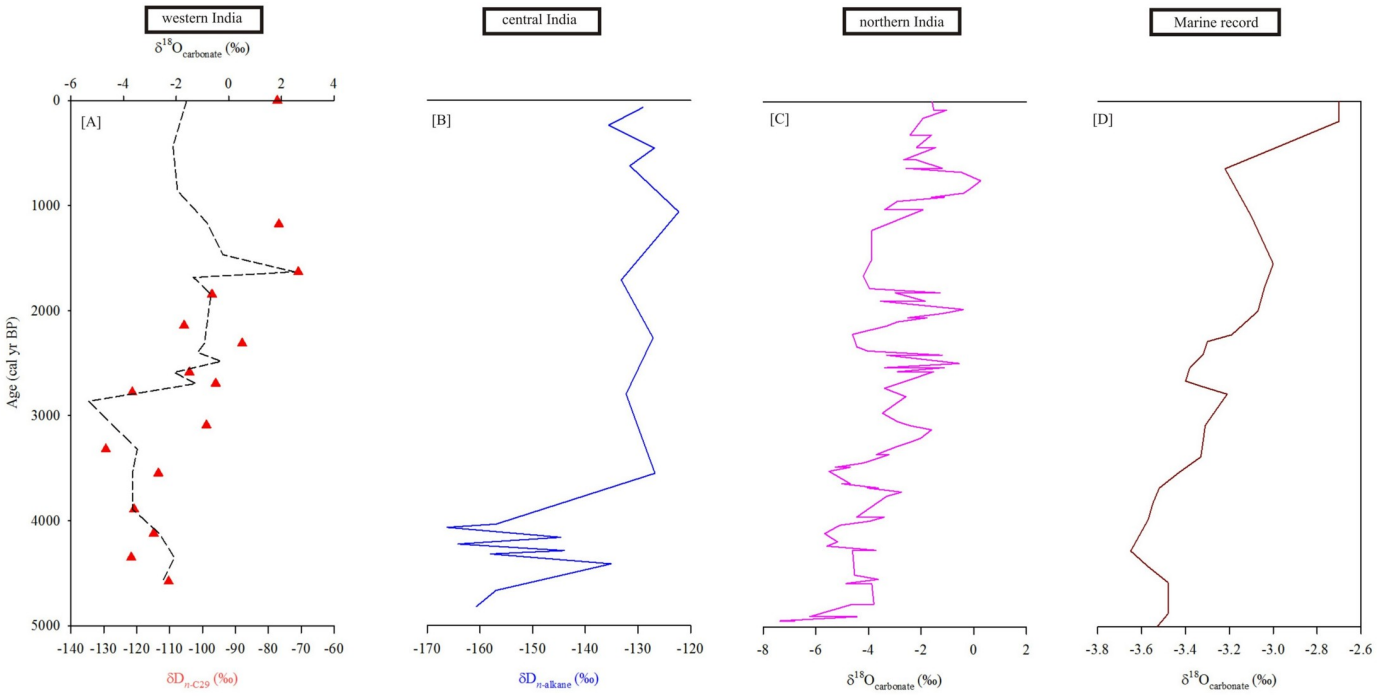

Fig 6. Compilation of the Mid-Late Holocene records from Indian monsoon realm. (A) δD_{C29} record from Banni region (this study) (B) δD record from Lonar Lake, central India [42], (C) $\delta^{18}O_{carbonate}$ from Tso Moriri lake, NW Himalayas [11], and (D) $\delta^{18}O_{carbonate}$ from northern Bay of Bengal [82].

https://doi.org/10.1371/journal.pone.0212743.g006

agreement with the record based on $\delta^{13}C$ values of sedimentary leaf waxes from the core monsoon zone of India [9], and mineralogical and isotopic investigation on core sediments from Lonar lake, central India [10, 80]. This humid phase also matches with the geochemical investigations of core sediments retrieved from continental shelf in eastern India [81].

The onset of aridity in the Banni region after 2500 cal yr BP was in phase with lowering of the sea-level during 2825 and 1835 cal yr BP, as observed from the Saurashtra coast in western India [76]. The results are also in line with the high resolution record from NW India: Nal Sarovar lake [77]; Pariyaj Lake [74], Lunkaransar and Didwana lakes [78, 79]. The onset of aridity after 3 ka is also inferred in a tidal terrace sequence at the mouth of the Kharod River in western India [83]. A stalagmite record from peninsular India also indicates an abrupt climate change characterized by the decline of ISM around 2800 yr BP [84]. The findings of drier conditions in Banni region during ca. 2500–1000 cal yr BP is good accordance with the pollen record from NE India [85]; sedimentary leaf waxes from core monsoon zone [9] and geochemical data from eastern India [81]. More positive $\delta D_{n\text{-alkane}}$ values of the Lonar lake sediments (central India) also provide evidences of the Late Holocene arid conditions (Fig 6B). The $\delta^{18}O$ values of the carbonates from the Tso Moriri lake, northern India also demonstrates a decline in the intensity of ISM precipitation during the Late Holocene (Fig 6C). Our record from Banni grassland is also in line with the climatic reconstruction from northern Bay of Bengal [82] that confirms a gradual decrease in the ISM intensity during the Late Holocene (Fig 6D).

The record from the Banni grasslands matches with the evidence of precipitation changes and vegetation responses in the other tropical grasslands across the globe. For instance, terrestrial ecosystems in the Sahara responded to the weakening of African monsoon during the Mid-Late Holocene by a conspicuous reduction in tropical trees from nearly 4300 cal yr BP to the establishment of current day desert ecosystem by ca. 2700 cal yr BP [86]. Studies from the

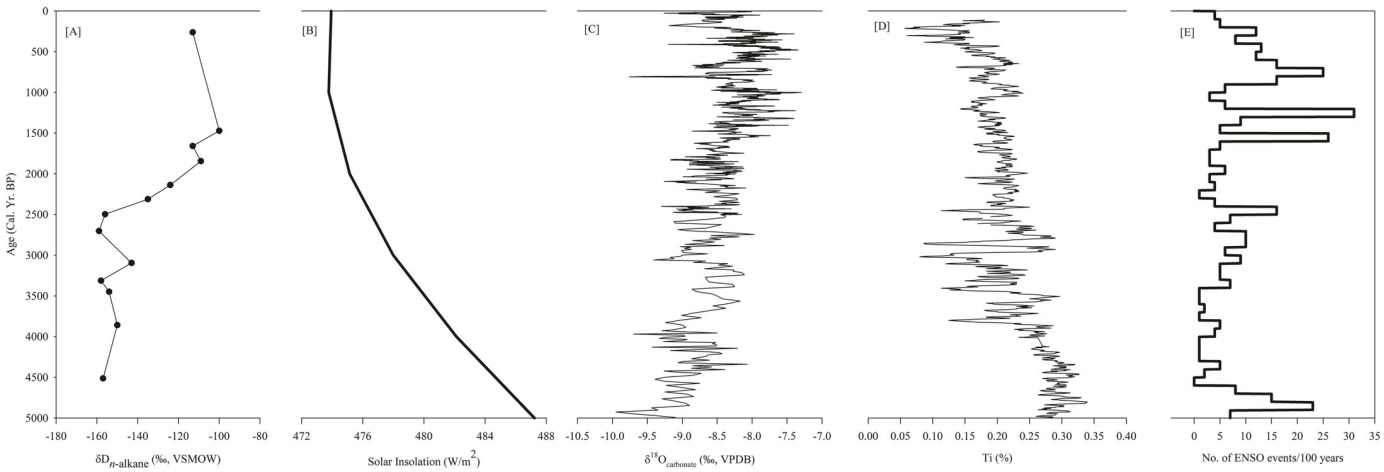

Fig 7. Compilation of Mid-Late Holocene records of terrestrial records across different monsoonal domains and forcing factors. (A) δD_{C29} record from Banni region (this study), (B) $\delta^{18}O_{carbonate}$ from Heshang cave, EASM [96], (C) $\delta^{18}O_{carbonate}$ from Liang Luar, AISM [90], (D) solar insolation curve from the northern hemisphere [91] and (E) frequency of ENSO activities [94].

https://doi.org/10.1371/journal.pone.0212743.g007

Manga Grasslands in northeastern Nigeria have also shown that climate was the major determinant of vegetation change during the Mid-Late Holocene with a shift towards more arid conditions until 1000 cal yr BP followed by wetter conditions towards the present [87]. Distinct biostratigraphical and sedimentological evidences of the shift towards drier climatic conditions during the Mid-Late Holocene were reported from multiple sites across Western Africa [88].

Teleconnections governing long-term regional climate variability

As various components of the different monsoon systems are interconnected through feedback mechanisms, perturbation of any of those components can affect the global monsoonal circulation [89]. For instance, less boreal summer monsoonal precipitation is linked with the increased Australian-Indonesian summer monsoonal (AISM) precipitation [90]. Therefore, understanding of land-ocean-atmosphere interaction on a global scale requires quantitative data from different monsoon domains. Towards this, climate records from different monsoonal domains (Fig 7) have been compared in this study to understand the role of forcing factors that persist across Hemispheres. The mean δD_{C29} values of the Chachi core sediments are significantly different for the phase-1 and 2, and this difference is correlated with the mean position of the ITCZ which is driven by the solar insolation [91] (Fig 7D). Monsoonal precipitation in the Northern Hemisphere increases with northward migration of ITCZ, accompanying decreased precipitation in the Southern Hemisphere; and vice versa [92]. Paleoclimatic records showed that the Southern Hemisphere insolation became more seasonal compared to Northern Hemisphere in the Late Holocene. The mean position of ITCZ during the phase-2 is thus postulated as the driving mechanism for the drying trend in ISM and East Asian summer monsoon dominated region and wet condition in the Southern Hemisphere (Fig 7A and 7D).

Increasing ENSO activity couldn also be argued for the increase in the δD_{C29} values after 2500 cal yr BP. An investigation based on the modern instrumental record suggested that majority of droughts in the ISM dominated regions are linked with the warm phases of ENSO events (i.e., El-Nino) [93]. The modern ENSO regime was established 3000 to 4500 cal yr BP and El-Nino events significantly increased after 2500 cal yr BP [94] concurrent with the marked dry condition in the Banni region (Fig 7E). This pattern in the precipitation correlates

well with the grain size data from EL Junco Crater Lake in the Galapagos Islands, inferred to reflect the higher frequency of El-Nino events [95]. Together position of ITCZ and ENSO activity appear to be linked to the inferred aridification in Banni region during the Late Holocene.

Conclusion

Climate-driven changes in grassland ecosystems of the Indian Summer Monsoon realm have been investigated, for the first time using the isotopic composition of biomarkers in lake sediments. After ca. 2500 cal yr BP, a gradual increase in the $\delta^{13}C_{n\text{-alkane}}$ values indicates the dominance of C_4 grasses at the expense of C_3 plants. Difference between the $\delta^{13}C_{n\text{-alkane}}$ values indicates that each *n*-alkane homologue had different C_3-C_4 proportional contributions. In the lake sediments, C_{29} and C_{31} homologues were mainly derived from C_3 plants and C_4 grasses respectively. The present study has used the δD_{C29} values as a proxy of the isotopic composition of paleoprecipitation. Meteorological and modeling observations show that δD values of modern precipitation in the Banni region are inversely related to the precipitation amount. This 'amount effect' based reconstruction suggests a marked decrease in the ISM precipitation after 2500 cal yr BP. The observed precipitation pattern in the climate record from Banni region corresponds well with published records. Coupled influence of southward migration of ITCZ and higher frequency of warm ENSO events led to the decrease in the ISM precipitation after 2500 cal yr BP and helped in establishing the grassland ecosystems.

Supporting information

S1 Fig. Representative distribution of *n*-alkanes from the modern vegetation (trees and grasses) in Banni region. Pr and Ph represent the concentration of pristane and phytane isoprenoids in the vegetation.
(JPG)

S2 Fig. Representative distribution of long-chain *n*-alkanes derived from Chachi core sediments. Pr and Ph represent the concentration of pristane and phytane isoprenoids in the sediments.
(JPG)

S3 Fig. The dotted line represents the variations in the %Char in the Banni grassland for the last 4600 cal yr BP. The values of %Char has been taken from Pillai et al., 2017. The dashed line represents the variability of pCO_2 concentration. The source of pCO_2 dataset is Lüthi et al., 2008.
(JPG)

S1 Table. The $\%C_4$ plants for the last 4600 cal yr BP has been estimated using bulk $\delta^{13}C_{org}$, $\delta^{13}C_{C29}$ and $\delta^{13}C_{C31}$ values from the Chachi core sediments. Numbers in bold represent outliers.
(DOCX)

Acknowledgments

SB gratefully acknowledges Mr. Mahesh Ghosh and Mr. Biswajit Giri for their assistance during the sample analyses. PS gratefully acknowledge financial support from the Department of Science and Technology, New Delhi (Project No. SB/S4/ES-684/2013). There was no additional external funding received for this study. We gratefully acknowledge the contribution from Padmasini Behra and Subhadeep Rakshit for their field assistance. We also thank Prof.

Yoshimura for his support to extract data from IsoGSM2 model. We are thankful to academic editor Prof. Hilton and the reviewers for their critical and thoughtful comments which helped to improve the quality of the manuscript.

Author Contributions

Conceptualization: Anusree A. S. Pillai, Anoop Ambili.

Data curation: Prasanta Sanyal, Anusree A. S. Pillai.

Formal analysis: Sayak Basu, Anusree A. S. Pillai, Anoop Ambili.

Funding acquisition: Prasanta Sanyal.

Investigation: Sayak Basu, Anusree A. S. Pillai, Anoop Ambili.

Methodology: Sayak Basu, Prasanta Sanyal, Anusree A. S. Pillai.

Resources: Prasanta Sanyal.

Supervision: Anoop Ambili.

Validation: Sayak Basu.

Visualization: Sayak Basu.

Writing – original draft: Sayak Basu.

Writing – review & editing: Prasanta Sanyal, Anoop Ambili.

References

1. Whittaker RH, Likens GE. The biosphere and man. Primary productivity of the biosphere Springer, Berlin, Heidelberg. 1975; 305–328.
2. Lieth H. Patterns of primary production in the biosphere. Dowden, Hutchinson & Ross. 1978.
3. Grace J, José JS, Meir P, Miranda HS, Montes RA. Productivity and carbon fluxes of tropical savannas. Journal of Biogeography. 2006; 33(3): 387–400.
4. Mix HT, Winnick MJ, Mulch A, Chamberlain CP. Grassland expansion as an instrument of hydrologic change in Neogene western North America. Earth and Planetary Science Letters. 2013; 377: 73–83.
5. Shanahan TM, Overpeck JT, Wheeler CW, Beck JW, Pigati JS, Talbot MR, et al. Paleoclimatic variations in West Africa from a record of late Pleistocene and Holocene lake level stands of Lake Bosumtwi, Ghana. Palaeogeography, Palaeoclimatology, Palaeoecology. 2006; 242: 287–302.
6. Veldman JW, Buisson E, Durigan G, Fernandes GW, Le Stradic S, Mahy G, et al. Toward an old-growth concept for grasslands, savannas, and woodlands. Frontiers in Ecology and the Environment. 2015; 13 (3): 154–162.
7. Sheffield J, Wood EF. Projected changes in drought occurrence under future global warming from multi-model, multi-scenario, IPCC AR4 simulations. Climate Dynamics. 2008; 31: 79–105.
8. Craine JM, Ocheltree TW, Nippert JB, Towne EG, Skibbe AM, Kembel S, et al. Global diversity of drought tolerance and grassland climate-change resilience. Nature Climate Change. 2013; 3: 63–67.
9. Ponton C, Giosan L, Eglinton TI, Fuller DQ, Johnson JE, Kumar P, et al. Holocene aridification of India. Geophysical Research Letters. 2012; 39: 1–6.
10. Prasad S, Anoop A, Riedel N, Sarkar S, Menzel P, Basavaiah N, et al. Prolonged monsoon droughts and links to indo-Pacific warm pool: A Holocene record from Lonar Lake, central India. Earth and Planetary Science Letters. 2014; 391: 171–182.
11. Mishra PK, Prasad S, Anoop A, Plessen B, Jehangir A, Gaye B, et al. Carbonate isotopes from high altitude Tso Moriri Lake (NW Himalayas) provide clues to late glacial and Holocene moisture source and atmospheric circulation changes. Palaeogeography, Palaeoclimatology, Palaeoecology. 2015; 425: 76–83.
12. Pillai AAS, Anoop A, Sankaran M, Sanyal P, Jha DK, Ratnam J, et al. Mid-late Holocene vegetation response to climatic drivers and biotic disturbances in the Banni grasslands of western India. Palaeogeography, Palaeoclimatology, Palaeoecology. 2017; 485: 869–878.

13. Pillai AAS, Anoop A, Prasad V, Manoj MC, Varghese S, Sankaran M, et al. Multi-proxy evidence for an arid shift in the climate and vegetation of the Banni grasslands of western India during the mid to late Holocene. Holocene. Forthcoming 2018
14. Krull E, Skjemstad J, Graetz D, Grice J, Dunning W, Cook G, et al. ^{13}C depleted charcoal from C_4 grasses and the role of occluded gases in phytolith. Organic Chemistry. 2003; 34: 1337–1352.
15. Wiesenberg GLB, Lehndorff E, Schwark L. Thermal degradation of rye and maize straw: lipid pattern changes as a function of temperature. Organic Geochemistry. 2009; 40: 167–174.
16. Basu S, Anoop A, Sanyal P, Singh P. Lipid distribution in the lake Ennamangalam, south India: Indicators of organic matter sources and paleoclimatic history. Quaternary International. 2017; 443: 238–247.
17. Leng MJ, Marshall JD. Palaeoclimate interpretation of stable isotope data from lake sediment archives. Quaternary Science Reviews. 2004; 23: 811–831.
18. Gujarat Institute of Desert Ecology (GUIDE). Status of Banni Grassland and Exigency of Restoration Efforts. Report. Vadodara: Gujarat Ecology Commission. 1998.
19. Joshi PN, Kumar V, Koladiya M, Patel YS, Karthik T. Local perceptions of grassland change and priorities for conservation of natural resources of Banni, Gujarat, India. Frontiers of Biology in China. 2010; 4: 549–556.
20. Kar A. Geomorphology of the Arid Lands of Kachchh and its importance in land resources planning. Landforms Processes & Environment Management. ACB Publications, Kolkota. 2011; 388–414.
21. Roy B. Pattern and causes of inundation of Rann of Kutch, Ph.D. Dissertation, M.S. University of Baroda, India. 1973; 170.
22. Maurya DM, Chowksey V, Patidar AK, Chamyal LS. A review and new data on neotectonic evolution of active faults in the Kachchh Basin, Western India: legacy of post-Deccan Trap tectonic inversion. Geological Society, London, Special Publications. 2016; 445: SP445-7.
23. Singh N, Kar A. Characteristics of major soils of Banni mudflat in arid western India and their relationship with topography. Journal of arid environments. 2001; 48: 509–520.
24. Patel Y, Joshi PN. A floristic Inventory in the Banni region of Bhuj Taluka, Kachchh district, Gujarat (India). Indian Forester. 2011; 137: 1114–1121.
25. Joshi PN, Kumar V, Koladiya M, Patel YS, Karthik T. Local perceptions of grassland change and priorities for conservation of natural resources of Banni, Gujarat, India. Frontiers of Biology in China. 2009; 4 (4): 549.
26. Ankit Y, Mishra PK, Kumar P, Jha DK, Kumar VV, Ambili V, et al. Molecular distribution and carbon isotope of n-alkanes from Ashtamudi Estuary, South India: Assessment of organic matter sources and paleoclimatic implications. Marine Chemistry. 2017; 196: 62–70.
27. Ghosh S, Sanyal P, Kumar R. Evolution of C4 plants and controlling factors: Insight from n-alkane isotopic values of NW Indian Siwalik paleosols. Organic Geochemistry. 2017; 110: 110–121.
28. Hou J, D'Andrea WJ, Liu Z. The influence of ^{14}C reservoir age on interpretation of paleolimnological records from the Tibetan Plateau. Quaternary Science Reviews. 2012; 48: 67–79.
29. Mischke S, Weynell M, Zhang C, Wiechert U. Spatial variability of 14C reservoir effects in Tibetan Plateau lakes. Quaternary International. 2013; 313: 147–155.
30. Mishra PK, Anoop A, Schettler G, Prasad S, Jehangir A, Menzel P, et al. Reconstructed late Quaternary hydrological changes from Lake Tso Moriri, NW Himalaya. Quaternary International. 2015; 371: 76–86.
31. Beuning KR, Talbot MR, Kelts K. A revised 30,000-year paleoclimatic and paleohydrologic history of Lake Albert, East Africa. Palaeogeography, Palaeoclimatology, Palaeoecology. 1997; 136(1–4): 259–279.
32. Wolfe AP, Miller GH, Olsen CA, Forman SL, Doran PT, Holmgren SU. Geochronology of high latitude lake sediments. In Long-term environmental change in Arctic and Antarctic lakes Springer, Dordrecht. 2004; 19–52
33. Lougheed BC, Filipsson HL, Snowball I. Large spatial variations in coastal 14 C reservoir age—a case study from the Baltic Sea. Climate of the Past. 2013; 9(3): 1015–28.
34. Bronk Ramsey C, Lee S. Recent and Planned Developments of the Program OxCal. Radiocarbon. 2013; 55: 720–730.
35. Reimer PJ, Baillie MGL, Bard E, Bayliss A, Beck JW, Blackwell PG, et al. IntCal09 and Marine09 radiocarbon age calibration curves, 0–50,000 years cal BP. Radiocarbon. 2009; 51: 1111–1150.
36. Cranwell PA, Eglinton G, Robinson N. Lipids of aquatic organisms as potential contributors to lacustrine sediments. Organic Geochemistry. 1987; 11: 513–527.
37. D'Anjou RM, Wei JH, Castañeda IS, Brigham-Grette J, Petsch ST, Finkelstein DB, et al. High-latitude environmental change during MIS 9 and 11: biogeochemical evidence from Lake El'gygytgyn, Far East Russia, Climate of the Past. 2013; 9: 567–581.

38. Eglinton G, Hamilton RJ. Leaf epicuticular waxes. Science. 1967; 156: 1322–1335. PMID: 4975474

39. Ficken KJ, Li B, Swain DL, Eglinton G. An n-alkane proxy for the sedimentary input of submerged/floating freshwater aquatic macrophytes. Organic Geochemistry. 2000; 31: 745–749.

40. Silliman JE, Meyers PA, Bourbonniere RA. Record of postglacial organic matter delivery and burial in sediments of Lake Ontario. Organic Geochemistry. 1996; 24: 463–472.

41. Poynter JG, Eglinton G. Molecular composition of three sediments from hole 717C: The Bengal Fan. Proceedings of the Ocean Drilling Program Scientific Results. 1990; 116: 155–161.

42. Sarkar S, Prasad S, Wilkes H, Riedel N, Stebich M, Basavaiah N, et al. Monsoon source shifts during the drying mid-Holocene: Biomarker isotope based evidence from the core 'monsoon zone' (CMZ) of India. Quaternary Science Reviews. 2015; 123: 144–157.

43. Yoshimura K, Kanamitsu M, Noone D, Oki T. Historical isotope simulation using reanalysis atmospheric data. Journal of Geophysical Research: Atmospheres. 2008; 113: D19108.

44. Claessens M, De Meester S, Van Landuyt L, De Clerck K, Janssen CR. Occurrence and distribution of microplastics in marine sediments along the Belgian coast. Marine Pollution Bulletin. 2011; 62(10): 2199–204. https://doi.org/10.1016/j.marpolbul.2011.06.030 PMID: 21802098

45. Hockun K, Mollenhauer G, Ho SL, Hefter J, Ohlendorf C, Zolitschka B et al. Using distributions and stable isotopes of n-alkanes to disentangle organic matter contributions to sediments of Laguna Potrok Aike, Argentina. Organic Geochemistry. 2016; 102: 110–119.

46. Wynn JG, and Bird MI. C4-derived soil organic carbon decomposes faster than its C3 counterpart in mixed C3/C4 soils. Global Change Biology. 2007; 13: 2206–2217.

47. Tipple BJ, Meyers SR, Pagani M. Carbon isotope ratio of Cenozoic CO_2: A comparative evaluation of available geochemical proxies. Paleoceanography. 2010; 25: 1–11.

48. Basu S, Agrawal S, Sanyal P, Mahato P, Kumar S, Sarkar A, et al. Carbon isotopic ratios of modern C_3-C_4 plants from the Gangetic plain, India and its implications to paleovegetational reconstruction. Palaeogeography, Palaeoclimatology, Palaeoecology. 2015; 440: 22–32.

49. Tierney JE, Russell JM, Huang Y, Damsté JSS, Hopmans EC, Cohen AS. Northern hemisphere controls on tropical southeast African climate during the past 60,000 years. Science. 2008; 322(5899): 252–255. https://doi.org/10.1126/science.1160485 PMID: 18787132

50. Niedermeyer EM, Schefuß E, Sessions AL, Mulitza S, Mollenhauer G. Orbital-and millennial scale changes in the hydrologic cycle and vegetation in the western African Sahel: insights from individual plant wax δD and $\delta^{13}C$. Quaternary Science Reviews. 2010; 29: 2996–3005.

51. Schefuß E, Kuhlmann H, Mollenhauer G, Prange M, Patzold J. Forcing of wet phases in southeast Africa over the past 17,000 years. Nature. 2011; 480: 509–512. https://doi.org/10.1038/nature10685 PMID: 22193106

52. Polissar PJ, Freeman KH. Effects of aridity and vegetation on plant-wax δD in modern lake sediments. Geochimica et Cosmochimica Acta. 2010; 74: 5785–5797.

53. Garcin Y, Schwab VF, Gleixner G, Kahmen A, Todou G, Sene O, et al. Hydrogen isotope ratios of lacustrine sedimentary n-alkanes as proxies of tropical African hydrology: insights from a calibration transect across Cameroon. Geochimica et Cosmochimica Acta. 2012; 79: 106–126.

54. Sachse D, Billault I, Bowen GJ, Chikaraishi Y, Dawson TE, Feakins SJ, et al. Molecular Paleohydrology: Interpreting the Hydrogen-Isotopic Composition of Lipid Biomarkers from Photosynthesizing Organisms. Annual Reviews of Earth and Planetary Sciences. 2012; 40: 221–249.

55. Liu W, Yang H, Li L. Hydrogen isotopic compositions of n-alkanes from terrestrial plants correlate with their ecological life forms. Oecologia. 2006; 150: 330–338. https://doi.org/10.1007/s00442-006-0494-0 PMID: 16977462

56. Smith FA, Freeman KH. Influence of physiology and climate on δD of leaf wax n-alkanes from C3 and C4 grasses. Geochimica et Cosmochimica Acta. 2006; 70: 1172–1187.

57. Pedentchouk N, Sumner W, Tipple B, Pagani M. $\delta^{13}C$ and δD compositions of n-alkanes from modern angiosperms and conifers: an experimental set up in central Washington State, USA. Organic Geochemistry. 2008; 39: 1066–1071.

58. McInerney FA, Helliker BR, Freeman KH. Hydrogen isotope ratios of leaf wax n-alkanes in grasses are insensitive to transpiration. Geochimica et Cosmochimica Acta. 2011; 75: 541–554.

59. Aichner B, Feakins SJ, Lee JE, Herzschuh U, Liu X. High-resolution leaf wax carbon and hydrogen isotopic record of the late Holocene paleoclimate in arid Central Asia. Climate of the Past. 2015; 11: 619–633.

60. Chikaraishi Y, Naraoka H. Carbon and hydrogen isotope variation of plant biomarkers in a plant-soil system. Chemical Geology. 2006; 231: 190–202.

61. Feakins SJ, Sessions AL. Controls on the D/H ratios of plant leaf waxes from an arid ecosystem. Geochimica et Cosmochimica Acta. 2010; 74: 2128–2141.

62. Günther F, Aichner B, Siegwolf R, Xu BQ, Yao T, Gleixner G, et al. A synthesis of hydrogen isotope variability and its hydrological significance at the Qinghai-Tibetan Plateau. Quaternary International. 2013; 313: 3–16.

63. Wang YV, Larsen T, Leduc G, Andersen N, Blanz T, Schneider EE. What does leaf wax δD from a mixed C_3/C_4 vegetation region tell us? Geochimica et Cosmochimica Acta. 2013; 111: 128–139.

64. Aichner B, Feakins SJ, Lee JE, Herzschuh U, Liu X. High resolution leaf wax carbon and hydrogen isotopic record of late Holocene paleoclimate in arid Central Asia. Climate of the Past Discussions. 2014; 10(6): 619.

65. Krull E, Sachse D, Mugler I, Thiele A, Gleixner G. Compound-specific $\delta^{13}C$ and $\delta^{2}H$ analyses of plant and soil organic matter: A preliminary assessment of the effects of vegetation change on ecosystem hydrology. Soil Biology and Biochemistry. 2006; 38: 3211–3221.

66. Polissar PJ, Freeman KH, Rowley DB, McInerney FA, Currie BS. Paleoaltimetry of the Tibetan Plateau from D/H ratios of lipid biomarkers. Earth and Planetary Science Letters. 2009; 287: 64–76.

67. Shanahan TM, McKay NP, Hughen KA, Overpeck JT, Otto-Bliesner B, Heil CW, et al. The time-transgressive termination of the African Humid Period. Nature Geoscience. 2015; 8(2): 140.

68. Dansgaard W. Stable isotopes in precipitation. Tellus. 1964; 16: 436–468.

69. Konecky BL, Russell JM, Johnson TC, Brown ET, Berke MA, Werne JP, et al. Atmospheric circulation patterns during late Pleistocene climate changes at Lake Malawi, Africa. Earth and Planetary Science Letters. 2011; 312: 318–326.

70. Bond WJ. What limits trees in C 4 grasslands and savannas? Annual Review of Ecology, Evolution, and Systematics. 2008; 39: 641–659.

71. Cerling TE, Harris JM, Macfadden BJ, Leakey MG, Quadek J, Eisenmann V, et al. Global vegetation change through the Miocene / Pliocene boundary. Nature. 1997; 389: 153–158.

72. Ferretti DF, Pendall E, Morgan JA, Nelson JA, LeCain D, Mosier AR. Partitioning evapotranspiration fluxes from a Colorado grassland using stable isotopes: Seasonal variations and ecosystem implications of elevated atmospheric CO_2. Plant Soil. 2003; 254: 291–303.

73. Oishi AC, Oren R, Stoy PC. Estimating components of forest evapotranspiration: A footprint approach for scaling sap flux measurements. Agricultural and Forest Meteorology. 2008; 148: 1719–1732.

74. Raj R, Chamyal LS, Prasad V, Sharma A, Tripathi JK, Verma P. Holocene climatic fluctuations in the Gujarat Alluvial Plains based on a multiproxy study of the Pariyaj Lake archive, western India. Palaeogeography, Palaeoclimatology, Palaeoecology. 2015; 421: 60–74.

75. Banerji US, Bhushan R, Jull AJ. Mid− late Holocene monsoonal records from the partially active mudflat of Diu Island, southern Saurashtra, Gujarat, western India. Quaternary International. 2017; 443: 200–210.

76. Banerji US, Pandey S, Bhushan R, Juyal N. Mid-Holocene climate and land—sea interaction along the southern coast of Saurashtra, western India. Journal of Asian Earth Sciences. 2015; 111: 428–439.

77. Prasad S, Kusumgar S, Gupta SK. A mid to late Holocene record of palaeoclimatic changes from Nal Sarovar: a palaeodesert margin lake in western India. Journal of Quaternary Science. 1997; 12(2): 153–159.

78. Wasson RJ, Smith GI, Agrawal DP. Late Quaternary sediments, minerals, and inferred geochemical history of Didwana Lake, Thar Desert, India. Palaeogeography, Palaeoclimatology, Palaeoecology. 1984; 46(4): 345–372.

79. Enzel Y, Ely LL, Mishra S, Ramesh R, Amit R, Lazar BR, et al. High-resolution Holocene environmental changes in the Thar Desert, northwestern India. Science. 1999; 284: 125–128. PMID: 10102808

80. Anoop A, Prasad S, Plessen B, Naumann R, Gaye B, Basavaiah N, et al. Palaeoenvironmental implications of evaporative Gaylussite crystals from Lonar lake, Central India. Journal of Quaternary Science. 2013; 28: 349–359.

81. Ankit Y, Kumar P, Anoop A, Mishra PK, Varghese S. Mid-late Holocene climate variability in the Indian monsoon: Evidence from continental shelf sediments adjacent to Rushikulya river, eastern India. Quaternary International. 2017; 443: 155–163.

82. Kudrass HR, Hofmann A, Doose H, Emeis K, Erlenkeuser H. Modulation and amplification of climatic changes in the Northern Hemisphere by the Indian summer monsoon during the past 80 ky. Geology. 2001; 29(1): 63–66.

83. Das A, Prizomwala SP, Makwana N, Thakkar MG. Late Pleistocene-Holocene climate and sea level changes inferred based on the tidal terrace sequence, Kachchh, Western India. Palaeogeography, Palaeoclimatology, Palaeoecology. 2017; 473: 82–93.

84. Sinha N, Gandhi N, Chakraborty S, Krishnan R, Yadava MG. and Ramesh R. Abrupt climate change at~ 2800 yr BP evidenced by a stalagmite record from peninsular India. The Holocene. 2018; p.0959683618788647.

85. Mazari RK, Bagati TN, Chauhan MS, Rajagopalan G. Palaeoclimatic record of last 2000 years in trans-Himalayan Lahaul-Spiti region. In Paleoclimate and Environmental Variability in Austral-Asian Transect during the Past 2000 Years, Proceedings, IGBP-PAGES/PEP II Symposium, Nagoya, Japan. 1996; 262–269.

86. Kröpelin S, Verschuren D, Lézine AM, Eggermont H, Cocquyt C, Francus P, et al. Climate-driven ecosystem succession in the Sahara: the past 6000 years. Science. 2008; 320: 765–768. https://doi.org/10.1126/science.1154913 PMID: 18467583

87. Holmes JA, Street-Perrott FA, Perrott RA, Stokes S, Waller MP, Huang Y, et al. Holocene landscape evolution of the Manga Grasslands, NE Nigeria: evidence from palaeolimnology and dune chronology. Journal of the Geological Society. 1999; 156(2): 357–368.

88. Salzmann U, Hoelzmann P, Morczinek I. Late Quaternary Climate and Vegetation of the Sudanian Zone of Northeast Nigeria. Quaternary Research. 2002; 58(1): 73–83.

89. Mohtadi M, Prange M, Steinke S. Palaeoclimatic insights into forcing and response of monsoon precipitation. Nature. 2016; 533(7602): 191.

90. Griffiths ML, Drysdale RN, Gagan MK, Frisia S, Zhao JX, Ayliffe LK, et al. Evidence for Holocene changes in Australian—Indonesian monsoon precipitation from stalagmite trace element and stable isotope ratios. Earth and Planetary Science Letters. 2010; 292(1–2): 27–38.

91. Berger A, Loutre MF. Insolation values for the climate of the last 10 million years. Quaternary Science Reviews. 1991; 10: 297–317

92. Baker PA, Seltzer GO, Fritz SC, Dunbar RB, Grove MJ, Tapia PM, et al. The history of South American tropical precipitation for the past 25,000 years. Science. 2001; 291(5504): 640–643 https://doi.org/10.1126/science.291.5504.640 PMID: 11158674

93. Varikoden H, Revadekar JV, Choudhary Y, Preethi B. Droughts of Indian summer monsoon associated with El Niño and Non-El Niño years. International Journal of Climatology. 2015; 35: 1916–1925.

94. Moy CM, Seltzer GO, Rodbell DT, Anderson DM. Variability of El Niño/Southern Oscillation activity at millennial timescales during the Holocene epoch. Nature. 2002; 420: 162. https://doi.org/10.1038/nature01194 PMID: 12432388

95. Conroy JL, Overpeck JT, Cole JE, Shanahan TM, Steinitz-Kannan M. Holocene changes in eastern tropical Pacific climate inferred from a Galápagos lake sediment record. Quaternary Science Reviews. 2008; 27(11): 1166–1180.

96. Hu C, Henderson GM, Huang J, Xie S, Sun Y, Johnson KR. Quantification of Holocene Asian monsoon precipitation from spatially separated cave records. Earth and Planetary Science Letters. 2008; 266(3–4): 221–32.